Synthesis of Ordered Microporous/Macroporous MOF-808 through Modulator-Induced Defect-Formation, and Surfactant Self-Assembly Strategies

Carolina Ardila-Suárez[1,2] ID *, Daniel R. Molina V.[3]* ID *, Halima Alem[4]* ID *, Víctor G. Baldovino-Medrano[2,5]* ID *, and Gustavo E. Ramírez-Caballero[1,2]** ID

1Grupo de Investigación en Polímeros, 2Centro de Investigaciones en Catálisis (@CICATUIS), 3Laboratorio de Resonancia Magnética Nuclear, and 5Laboratorio de Ciencia de Superficies (@Csss-UIS), all at Parque Tecnológico de Guatiguará (PTG), km 2 vía El Refugio, Universidad Industrial de Santander, Piedecuesta (Santander), 681011, Colombia. 4Université de Lorraine, CNRS, Institut Jean Lamour (IJL), UMR 7198, Nancy, France.

Content

1. Experimental Methods

1.1. Dissolution/H NMR Spectroscopy

We performed the analysis of as-synthesized and activated MOFs, according to previous work [1]. Thus, 600 μL of NaOH 1M in D_2O were added to 20 mg of each sample. The samples were digested for a period of 24 h. This procedure dissolves just the organic portion of the MOF, i.e., organic ligand, modulator agent, and solvent. The remaining ZrO2 sinks to the bottom, and it does not interfere with the analysis.

### 1.2. Spectrophotometric Determination of the CMC of CTAB

An Agilent/HP 8453 UV-Visible Spectrophotometer was employed for the calculation of the critical micelle concentration of CTAB, according to previous work[2]. The study was first performed in aqueous solutions with the aim of corroborating the accuracy of the methodology. Then, 5 CTAB aqueous solutions, i.e., 0.8, 0.60, 0.77, 0.99, 1.98 and 19.92 mM were prepared and 0.001 M of methylene blue was added to each solution. Subsequently, 8 solutions of CTAB in a DMF/Acetic Acid mixture (8:3 v/v), namely, 0.37, 0.56, 0.83, 1.20, 2.29, 4.34, 10.34 and 21.36 mM. The solutions absorbance was measured over a wavelength range of 400-600 nm, and a baseline correction was made using deionized water and the DMF/Acetic Acid mixture, respectively**.**

2. Results and Discussion

2.1. Thermal stability

Three different weight loss regions were identified, according to previous studies [3]. The use of different modulators during synthesis leads to changes in their resulting thermograms. Thus, according to the literature [4, 5], the more significant weight losses in the region I, are related to larger surface areas. In our case, the weight loss in this region follows the trend ZrBTC-F > ZrBTC-A > ZrBTC-P.

Consequently, the ZrBTC-F MOF, which exhibited the most significant weight loss in the region I, exhibited also the highest surface area. Furthermore, in region II, due to a similar temperature range of weight loss, is not possible to analyze separately two different events: the removal of the monocarboxylate linkers: formate, acetate, and propionate of ZrBTC-F, ZrBTC-A, and ZrBTC-P MOFs, respectively, and the dehydroxylation of the zirconium nodes. Moreover, there are also differences in region III of synthesized MOFs. Shearer et al. [1] studied the correlation between decomposition weight loss with the presence of missing linker defects, and accordingly, we performed a quantitative analysis of TGA data. The formula of the dehydroxylated MOF-808 is reported as Zr6O4(OH)4(BTC)2 [6] and, after combustion, the residue in the TGA experiments is assumed to be ZrO2, as presented in Equation 1 [7]. Thus, the expected weight loss for the decomposition, according to the stoichiometry, was calculated and then compared with the corresponding weight loss in the recorded thermograms.

$$Zr_6O_4(C_9H_3O_6)_2 + 17.5O_{2\,(g)} \rightarrow 6ZrO_2 + 18CO_{2\,(g)} + 3H_2O_{(g)}\ (1)$$
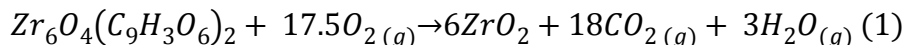
We performed a mass balance of the III region of the TGA thermogram. If we assume a base calculation of 100 g of the initial $Zr_6O_4(C_9H_3O_6)_2$ (MW=1025.57 g/mol), the mass of the solid residue 6 moles of ZrO_2 (739.34 g/mol) is consequently, 72.11 g. Then, the expected total weight loss would be ca. 27.89%. Accordingly, the ZrBTC-F, ZrBTC-A, and ZrBTC-P MOFs exhibited a decomposition weight loss magnitude of 19.54%, 23.23%, and 21.00%, respectively. These weight losses are lower than the theoretical defect-free behavior, which can be related to the partial deficiency of organic linkers that were replaced by modulators on the coordination of zirconium nodes. Moreover, the weight loss of the ZrBTC-F and ZrBTC-P materials are similar and lower than the resulting one of the ZrBTC-A MOF.
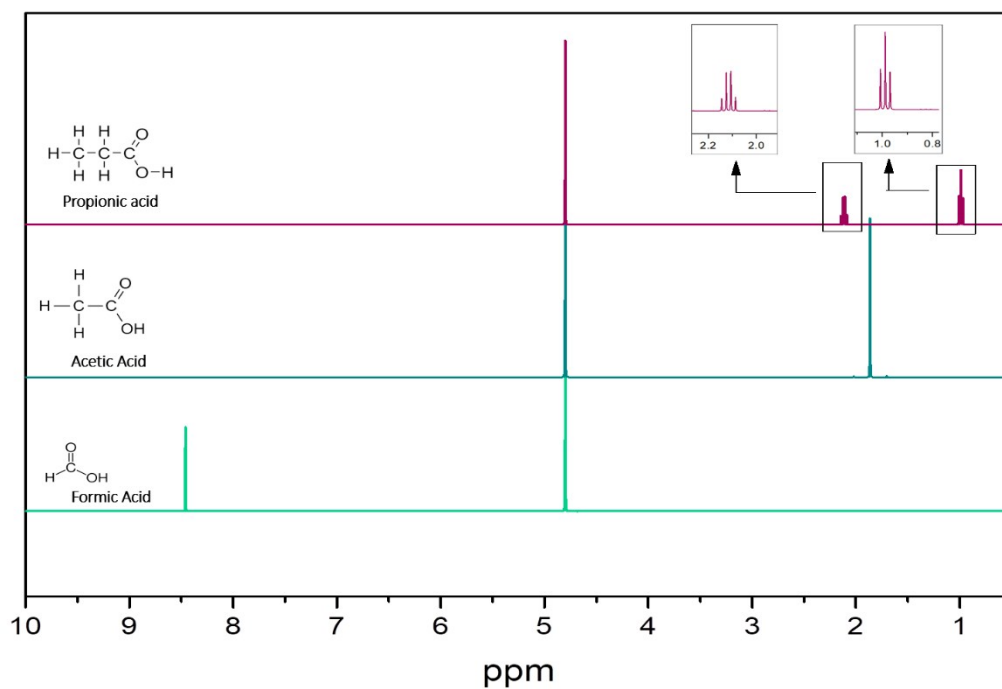
2.2. Dissolution/H NMR Spectroscopy

In general, the spectra recorded on the resulting MOFs after the digestion are clean. There are only the signals assigned to the dimethylamine, the BTC3-, formate, acetate, and propionate, See Figures S1 and S2. The ^{1}H NMR spectra recorded from the ZrBTC-F,

ZrBTC-A and ZrBTC-P samples after digestion are shown in Figures 5, S3, and S4, respectively. To determine if the monocarboxylates are indeed incorporated into the MOF -808 framework or just occluded in the pores as free acids, we recorded the spectra for the ZrBTC-A, ZrBTC-F, and ZrBTC-P MOFs before and after the activation process. Therefore, the monocarboxylates detected after the activation process are coordinated to the zirconium nodes. Moreover, all spectra recorded on the synthesized materials contain

As reported previously for the UiO-66 MOF [1], we calculated the molar ratios between the modulator and the BTC linker, $\frac{Modulator}{BTC}m_{r}$, before and after the activation process with the aim of compare quantitatively the concentration of modulator coordinated to the zirconium nodes. After activation, this ratio decreased 1.39 %, 1.38 %, and 0 % for ZrBTC-A, ZrBTC-F, and ZrBTC-P MOFs, respectively. Then, after activation, the molar ratio between each modulator and the BTC linker were 2.13, 1.43, and 2.03 for the ZrBTC-A, ZrBTC-F, and ZrBTC-P, respectively. Accordingly, the ZrBTC-F and ZrBTC-P materials exhibited similar and higher ratios compared to the ZrBTC-A MOFs. These results could be correlated to the fact that the ZrBTC-F and ZrBTC-P materials exhibited a larger percentage of microporous volume compared to the ZrBTC-A MOF, and this last, by the contrary, showed larger mesoporous volume than the other two materials. Furthermore, TGA results reflect that the weight loss percentage of ZrBTC-A, in the region associated with the decomposition of the organic linker, was more significant compared to the ZrBTC-F and ZrBTC-P MOFs. Probably, a low quantity of acetates was attached to the zirconium nodes, and instead, they formed clusters than favored the formation of large mesopores in ZrBTC-A MOF.
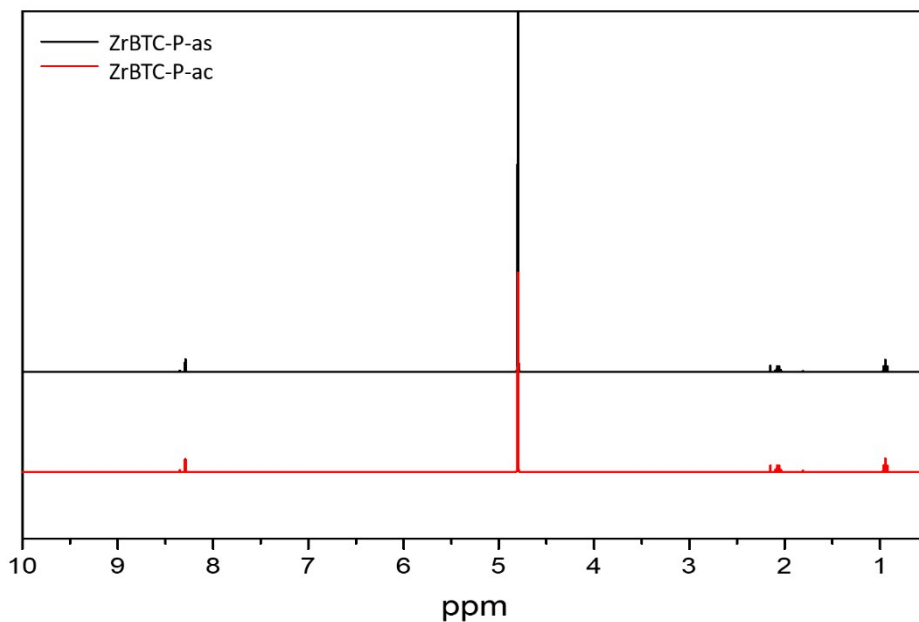
Figure S1. Dissolution/^{1}H NMR spectra obtained on the modulators using in this work.
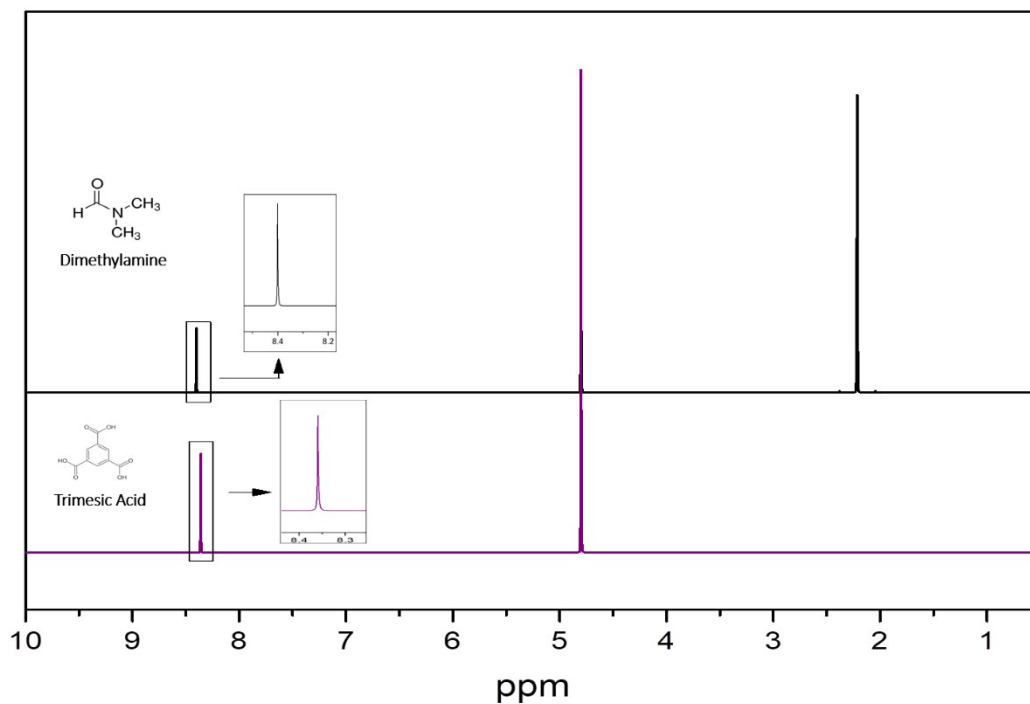
Figure S2. Dissolution/^{1}H NMR spectra obtained on dimethylamine (DMF hydrolysis product) and trimesic acid, BTC (organic ligand).
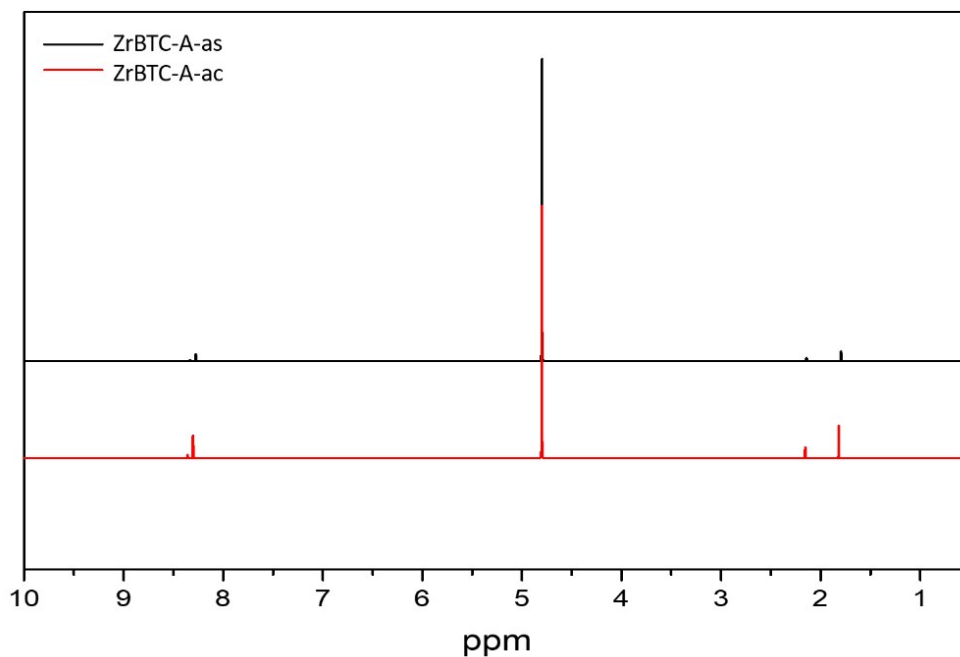
Figure S3. Dissolution/^{1}H NMR spectra obtained on the MOF synthesized using acetic acid as modulator before (ZrBTC-A-as) and after (ZrBTC-A-ac) the activation process.

Figure S4. Dissolution/^{1}H NMR spectra obtained on the MOF synthesized using propionic acid as modulator before (ZrBTC-P-as) and after (ZrBTC-P-ac) the activation process.

Formic Acid Modulation

ZrBTCF-as

$$\frac{Formic\ Acid}{BTC}m_r = \frac{Formic\ Acid\ Int.}{BTC\ Int.}\left(\frac{N_{H-BTC}}{N_{H-FA}}\right) = \left(\frac{0.72}{1.00}\right)\left(\frac{3}{1}\right) = 2.16$$

ZrBTCF-ac

$$\frac{Formic\ Acid}{BTC}m_r = \frac{Formic\ Acid\ Int.}{BTC\ Int.}\left(\frac{N_{H-BTC}}{N_{H-FA}}\right) = \left(\frac{0.71}{1.00}\right)\left(\frac{3}{1}\right) = 2.13$$

Acetic Acid Modulation

ZrBTCA-as

$$\frac{Acetic\ Acid}{BTC}m_r = \frac{Acetic\ Acid\ Int.}{BTC\ Int.}\left(\frac{N_{H-BTC}}{N_{H-AA}}\right) = \left(\frac{1.00}{0.69}\right)\left(\frac{3}{3}\right) = 1.45$$

$$\frac{Formic\ Acid}{BTC}m_r = \frac{Formic\ Acid\ Int.}{BTC\ Int.}\left(\frac{N_{H-BTC}}{N_{H-FA}}\right) = \left(\frac{0.11}{0.69}\right)\left(\frac{3}{1}\right) = 0.48$$

$$\frac{Modulators}{BTC}m_r = \frac{Formic\ Acid}{BTC} + \frac{Acetic\ Acid}{BTC} = 1.92$$

ZrBTCA-ac

$$\frac{Acetic\ Acid}{BTC}m_r = \frac{Acetic\ Acid\ Int.}{BTC\ Int.}\left(\frac{N_{H-BTC}}{N_{H-AA}}\right) = \left(\frac{1.00}{0.70}\right)\left(\frac{3}{3}\right) = 1.43$$

$$\frac{Formic\ Acid}{BTC}m_r = \frac{Formic\ Acid\ Int.}{BTC\ Int.}\left(\frac{N_{H-BTC}}{N_{H-FA}}\right) = \left(\frac{0.11}{0.70}\right)\left(\frac{3}{1}\right) = 0.48$$

$$\frac{Modulators}{BTC}m_r = \frac{Formic\ Acid}{BTC} + \frac{Acetic\ Acid}{BTC} = 1.91$$

Propionic Acid Modulation

- Triplet

ZrBTCP-as

$$\frac{Propionic\ Acid}{BTC}m_r = \frac{Propionic\ Int.}{BTC\ Int.}\left(\frac{N_{H-BTC}}{N_{H-PA}}\right) = \left(\frac{3.00}{1.48}\right)\left(\frac{3}{3}\right) = 2.03$$

$$\frac{Formic\ Acid}{BTC}m_r = \frac{Formic\ Acid\ Int.}{BTC\ Int.}\left(\frac{N_{H-BTC}}{N_{H-FA}}\right) = \left(\frac{0.19}{1.48}\right)\left(\frac{3}{1}\right) = 0.39$$

$$\frac{Modulators}{BTC}m_r = \frac{Formic\ Acid}{BTC} + \frac{Propionic\ Acid}{BTC} = 2.42$$

ZrBTCP-ac

$$\frac{Propionic\ Acid}{BTC}m_r = \frac{Propionic\ Acid\ Int.}{BTC\ Int.}\left(\frac{N_{H-BTC}}{N_{H-PA}}\right) = \left(\frac{3.00}{1.48}\right)\left(\frac{3}{3}\right) = 2.03$$

$$\frac{Formic\ Acid}{BTC}m_r = \frac{Formic\ Acid\ Int.}{BTC\ Int.}\left(\frac{N_{H-BTC}}{N_{H-FA}}\right) = \left(\frac{0.18}{1.48}\right)\left(\frac{3}{1}\right) = 0.37$$

$$\frac{Modulators}{BTC}m_r = \frac{Formic\ Acid}{BTC} + \frac{Propionic\ Acid}{BTC} = 2.40$$

- Quadruple

ZrBTCP-as

$$\frac{Propionic\ Acid}{BTC}m_r = \frac{Propionic\ Int.}{BTC\ Int.}\left(\frac{N_{H-BTC}}{N_{H-PA}}\right) = \left(\frac{2.00}{1.48}\right)\left(\frac{3}{2}\right) = 2.01$$

$$\frac{Formic\ Acid}{BTC}m_r = \frac{Formic\ Acid\ Int.}{BTC\ Int.}\left(\frac{N_{H-BTC}}{N_{H-FA}}\right) = \left(\frac{0.19}{1.48}\right)\left(\frac{3}{1}\right) = 0.38$$

$$\frac{Modulators}{BTC}m_r = \frac{Formic\ Acid}{BTC} + \frac{Propionic\ Acid}{BTC} = 2.39$$

ZrBTCP-ac

$$\frac{Propionic\ Acid}{BTC}m_r = \frac{Propionic\ Acid\ Int.}{BTC\ Int.}\left(\frac{N_{H-BTC}}{N_{H-PA}}\right) = \left(\frac{2.00}{1.48}\right)\left(\frac{3}{2}\right) = 2.03$$

$$\frac{Formic\ Acid}{BTC} m_r = \frac{Formic\ Acid\ Int.}{BTC\ Int.} \left(\frac{N_{H-BTC}}{N_{H-FA}}\right) = \left(\frac{0.18}{1.48}\right)\left(\frac{3}{1}\right) = 0.36$$

$$\frac{Modulators}{BTC} m_r = \frac{Formic\ Acid}{BTC} + \frac{Propionic\ Acid}{BTC} = 2.39$$

2.3. Crystallinity

The crystalline structure analysis done by powder X-ray diffraction showed that the materials synthesized have the previously reported set of reflections of MOF-808, i.e., $2\theta = 4.34°$ which was assigned to the (111) plane of MOF-808 and $2\theta = 8.32°$ and $8.69°$ which were assigned to diffraction from the planes (311) and (222), respectively. Although the ZrBTC-P material exhibited more defined peaks compared to the ZrBTC-F and ZrBTC-A MOFs, the three materials exhibited a certain degree of amorphicity, that could be related to their significant mesoporosity caused by missing linker defects. The synthesized materials crystallized in the cubic space group Fd3̄m, Table S1. The lattice parameters of the materials synthesized herein are very similar to the previously reported for MOF-808 and as postulated by Liang et al. [8]. The differences between them, according to the LeBail refinement results, could be related to the differences of solvent molecules that remain occluded inside the structure.

Table S1. Crystallinity data and structure refinement of the ZrBTC-F, ZrBTC-A, ZrBTC-P, ZrBTCAE-1, and ZrBTC-AE-2 material.

	Crystal system	Space group	Cell parameters (Å)	Volume (Å³)	Chi2
ZrBTC-F	Cubic	Fd3̄m	35.12450(329)	43334.152(70.47)	1.41
ZrBTC-A	Cubic	Fd3̄m	35.24473(210)	43780.695(45.20)	1.24
ZrBTC-P	Cubic	Fd3̄m	35.27621(150)	43887.953(32.44)	1.24
ZrBTCAE-1	Cubic	Fd3̄m	35.18252(106)	43549.270(22.87)	1.26
ZrBTCAE-2	Cubic	Fd3̄m	35.19824(81)	43607.660(17.45)	1.18
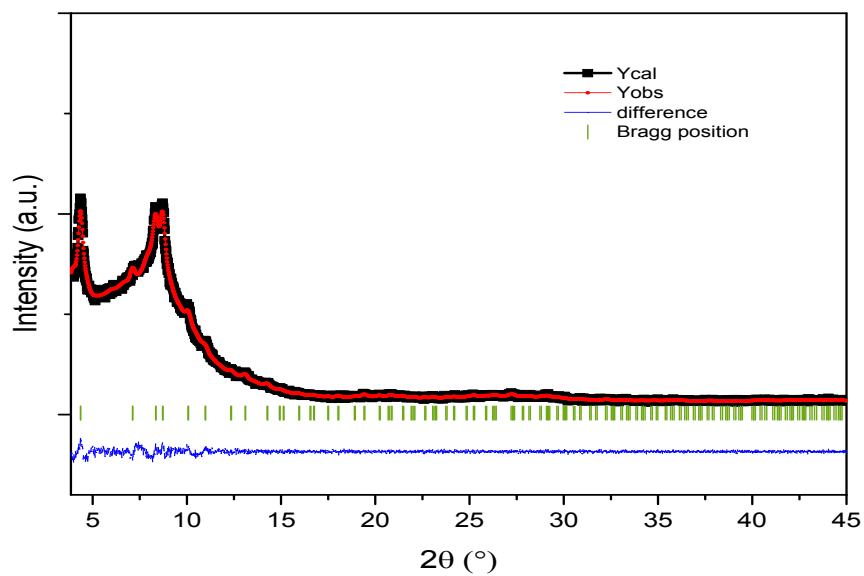
Figure S5. Le Bail profile fitting for ZrBTC-F, using experimental PXRD data. Experimental data is shown in red squares, the calculation in black, the difference in blue line, and Bragg reflection markers in green.
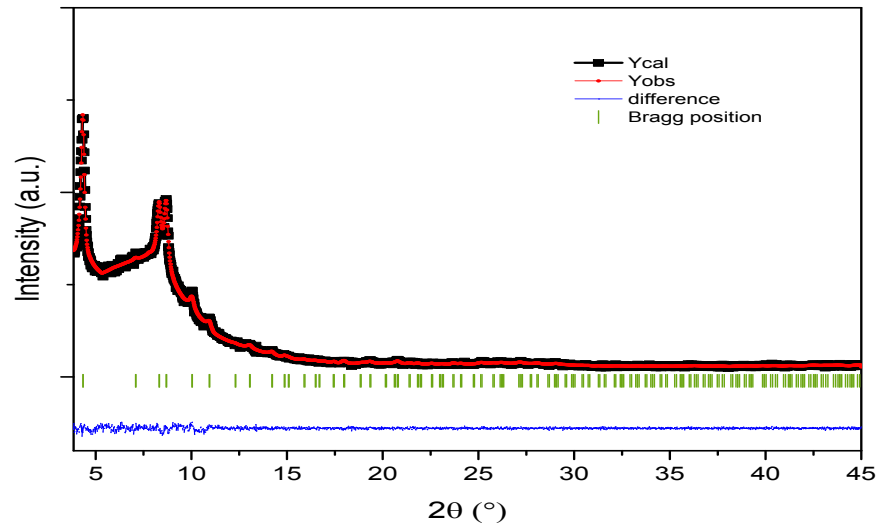
Figure S6. Le Bail profile fitting for ZrBTC-A, using experimental PXRD data. Experimental data is shown in red squares, the calculation in black, the difference in blue line, and Bragg reflection markers in green.
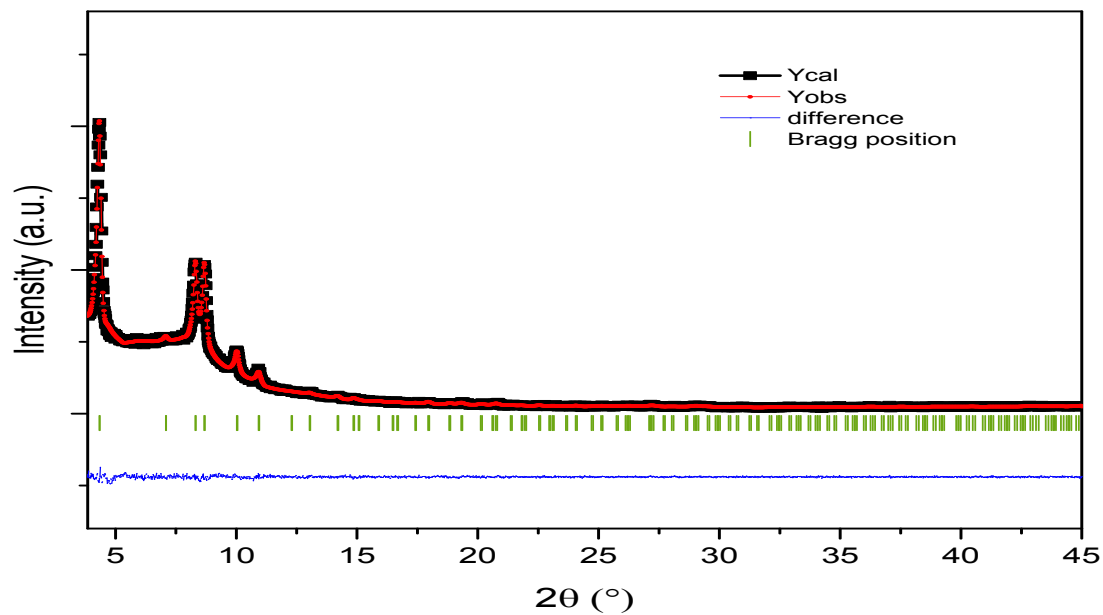
Figure S7. Le Bail profile fitting for ZrBTC-P, using experimental PXRD data. Experimental data is shown in red squares, the calculation in black, the difference in blue line, and Bragg reflection markers in green.
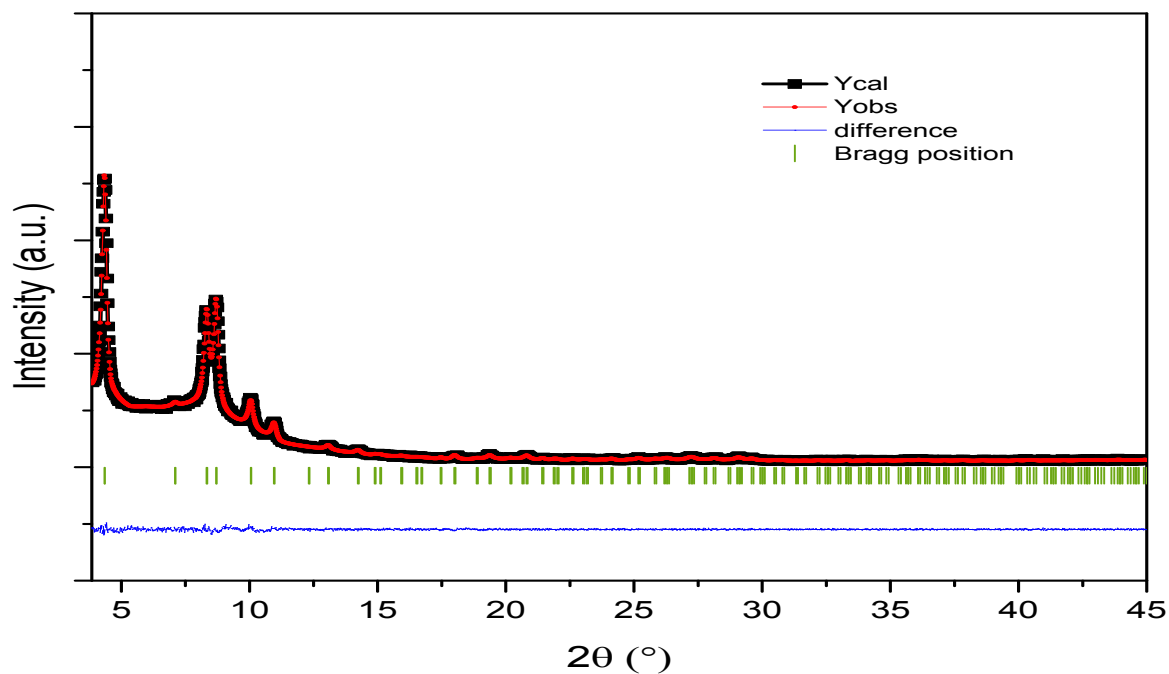
Figure S8. Le Bail profile fitting for ZrBTC-AE1, using experimental PXRD data. Experimental data is shown in red squares, the calculation in black, the difference in blue line, and Bragg reflection markers in green.

Figure S9. Le Bail profile fitting for ZrBTC-AE2, using experimental PXRD data. Experimental data is shown in red squares, the calculation in black, the difference in blue line, and Bragg reflection markers in green.
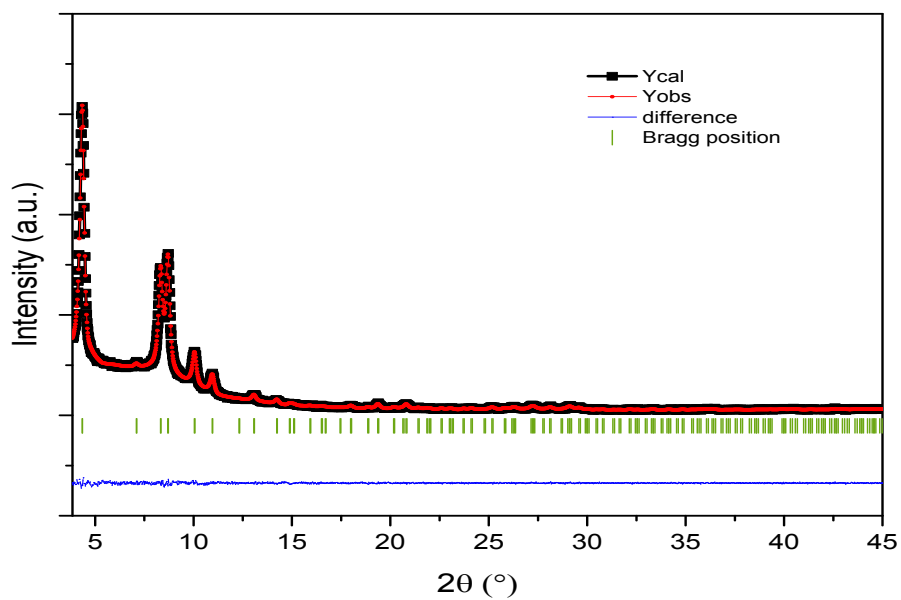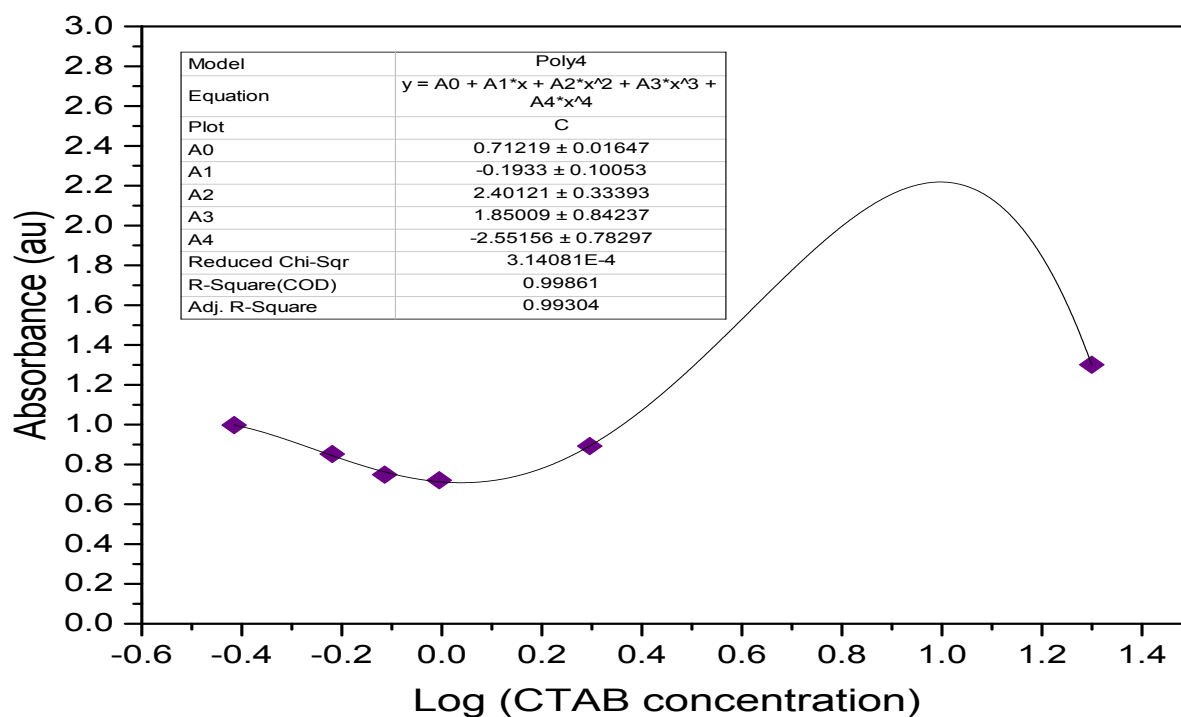
We followed the methodology of our previous work [9], assuming that the ZrBTC-AE2 material can represent a 100 % crystalline MOF-808. Hence, its XRD pattern was taken as a reference for the calculation of the degree of amorphicity of ZrBTCA-E1 and ZrBTC-A. Accordingly, the relative crystallinity of ZrBTC-AE1 and ZrBTC-A were 86 % and 59 %, respectively. The addition of CTAB during synthesis allows the formation of more ordered crystals of MOF-808.
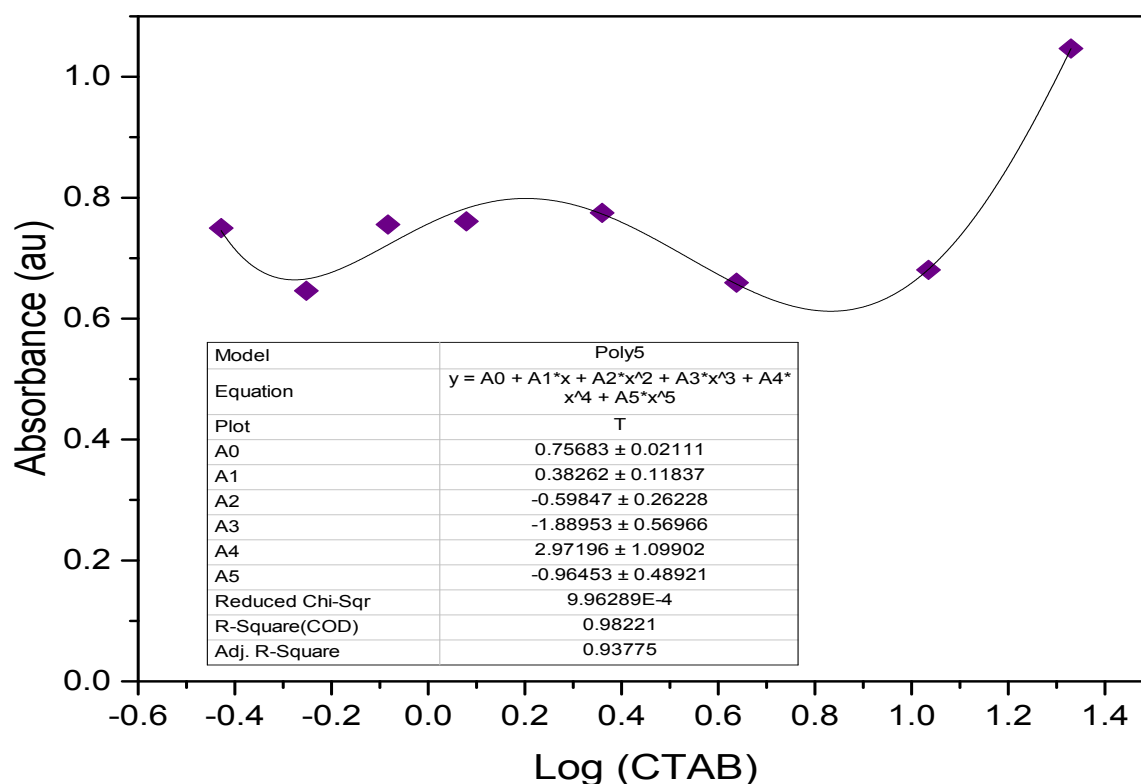
2.4. Spectrophotometric Determination of the CMC of CTAB

The maximum absorbance for each aqueous CTAB solution is observed at $\lambda = 397$ nm. These values were plotted and fitted according to Figure SX. After the calculation of the function minimum, the calculated CMC of CTAB is 1.1 mM, which is very similar to the previously reported CMC of 1 mM for CTAB in aqueous solutions [10].

Model	Poly4
Equation	$y = A0 + A1*x + A2*x^2 + A3*x^3 + A4*x^4$
Plot	C
A0	0.71219 ± 0.01647
A1	-0.1933 ± 0.10053
A2	2.40121 ± 0.33393
A3	1.85009 ± 0.84237
A4	-2.55156 ± 0.78297
Reduced Chi-Sqr	3.14081E-4
R-Square(COD)	0.99861
Adj. R-Square	0.99304

Figure S10. Plot showing the 4th order polynomial curve fit of the absorbance as a function of the CTAB concentration aqueous solutions, $\lambda = 397$ nm.

Accordingly, we performed the same experiment for the DMF/Acetic Acid mixture (8:3 v/v), which corresponds to the reaction mixture of the MOFs synthesis. In this case, two different absorbance maximums where detected: λ= 392 and 493 nm. The data collected for λ= 392 nm were plotted and fitted according to Figure S11. After the calculation of the function minimum, the calculated CMC of CTAB is 6.8 mM. This value is lower than the concentrations of CTAB, **13,02** and **26,037** mM, employed for the synthesis of ZrBTC-AE1 and ZrBTC-AE2, respectively. Thus, the CTAB concentrations employed during the MOFs synthesis induced its self-assembly for the formation of the micelles.

Model	Poly5
Equation	$y = A0 + A1*x + A2*x^2 + A3*x^3 + A4*x^4 + A5*x^5$
Plot	T
A0	0.75683 ± 0.02111
A1	0.38262 ± 0.11837
A2	-0.59847 ± 0.26228
A3	-1.88953 ± 0.56966
A4	2.97196 ± 1.09902
A5	-0.96453 ± 0.48921
Reduced Chi-Sqr	9.96289E-4
R-Square(COD)	0.98221
Adj. R-Square	0.93775

Figure S11. Plot showing the 5th order polynomial curve fit of the absorbance as a function of the CTAB concentration in the DMF/Acetic Acid mixture (8:3 v/v), λ= 397 nm.

2.5. Molecular structure

The bands around 1600 –1400 cm^{-1} are associated with the C-O of carboxylates linked to the metal centers. Further, the bands in the region of 1480–1420 cm^{-1} corresponded to the C=C in the aromatic compound of the organic linker [11]. The bands observed in the region of 750–655 cm^{-1} are related to the asymmetric vibration of the Zr-(μ_3-O) bridges in the framework building blocks. The band at 640 cm^{-1} is assigned to a vibration of the hexanuclear cluster, and the band around 545– 555 cm^{-1} is assigned to the Zr–(OC) asymmetric stretching vibration [12].

## 2.6. Surface chemistry

2.6.1. Surface chemical state by XPS

The empirical formulas were estimated on a hydrogen-free basis and according to our previous works [9, 13]: $CO_{0.843}Zr_{0.182}N_{0.001}Cl_{0.011}$, $CO_{1.002}Zr_{0.211}N_{0.003}Cl_{0.010}$, and $C_{O1.001}Zr_{0.203}N_{0.004}Cl_{0.014}$ for ZrBTC-F, ZrBTC-A, and ZrBTC-P, respectively. Related to the materials synthesized using surfactant, the empirical formulas were estimated as $CO_{0.961}Zr_{0.199}N_{0.001}$, and $CO_{0.956}Zr_{0.209}N_{0.003}Cl_{0.008}$ for ZrBTC-AE1, and ZrBTC-AE2, respectively. Compared to the previously reported formula $CO_{1.848}Zr_{0.25}H_{0.25}$ [6], the materials synthesized herein exhibited deficiencies at the surfaces of ca. 46% and 20%, respectively. These findings are in agreement with our previous discussion [9].

2.6.2. Chemical surface composition through ToF –SIMS
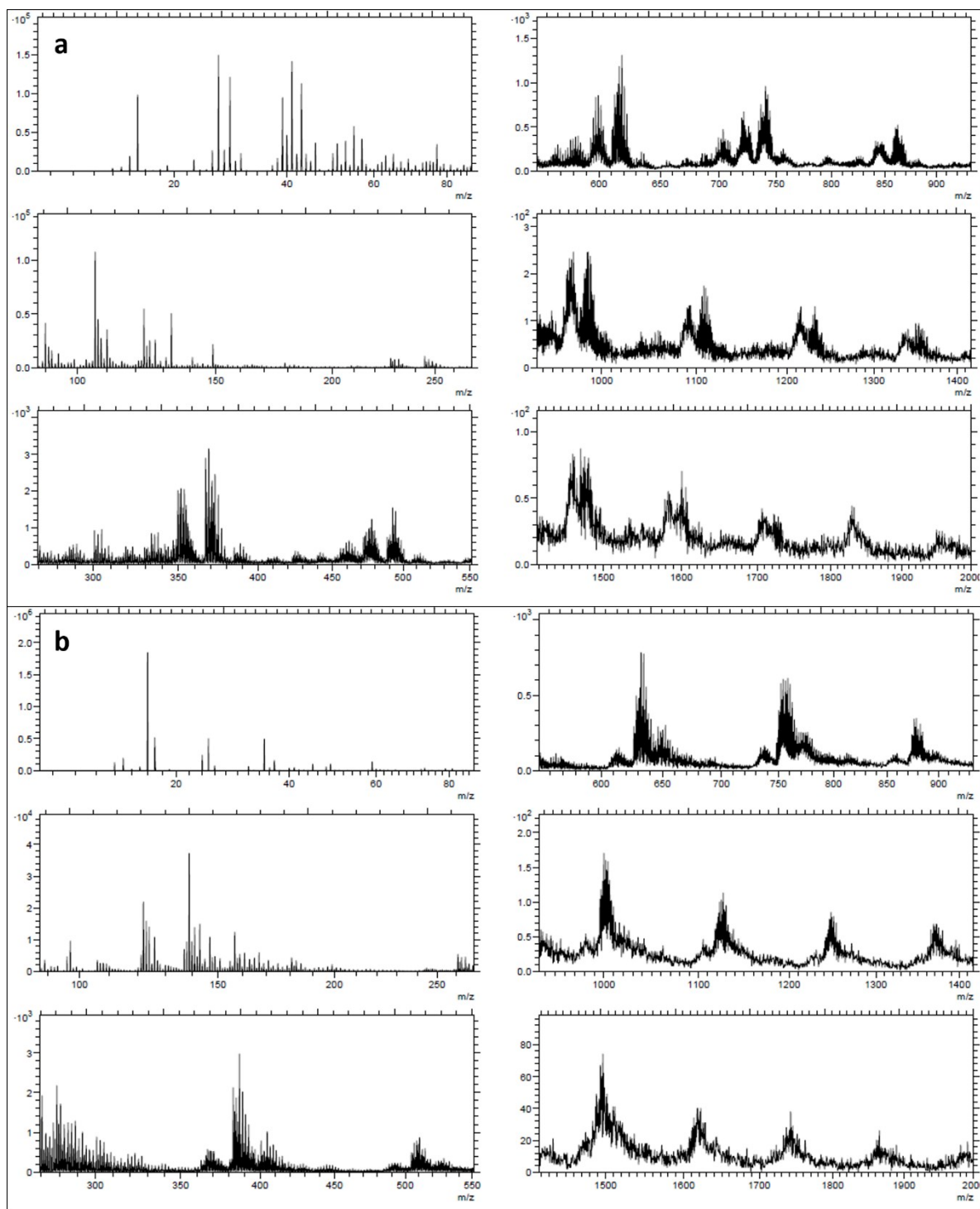
Figure S12. Spectra of the surface (a) Positive (b) Negative Secondary Ion Polarity of ZrBTC-AE2 MOF.
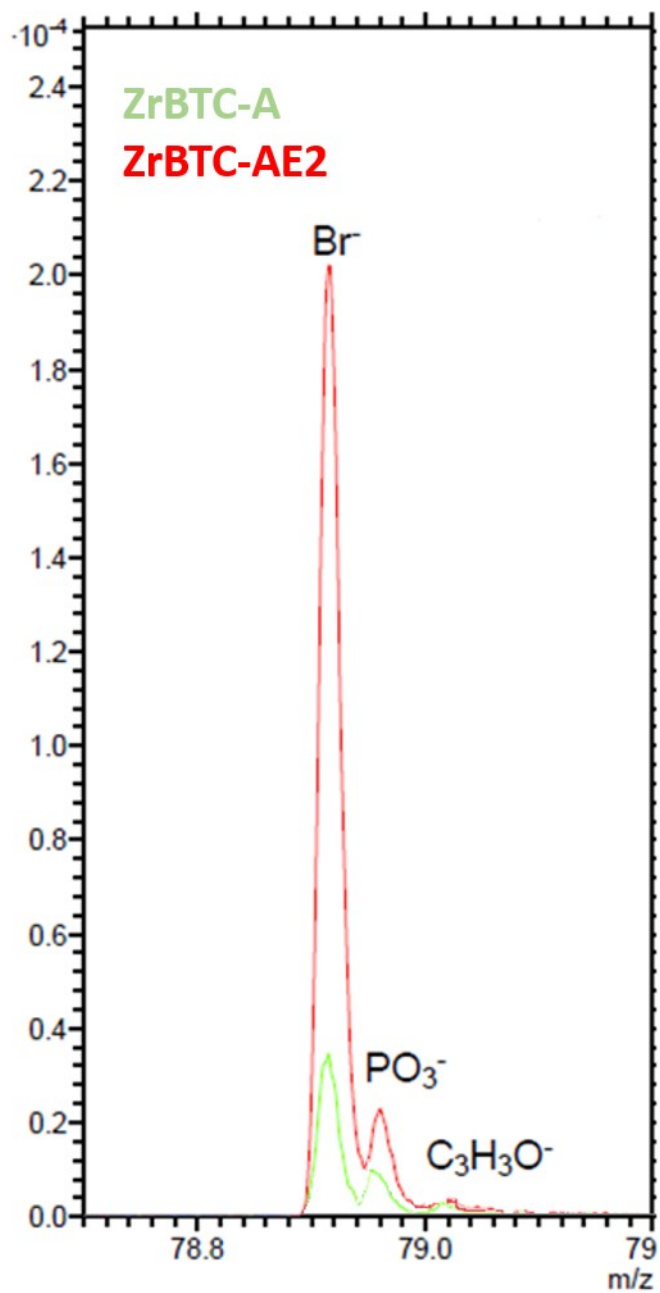
Figure S13. Spectra comparison of the surface Negative Secondary Ion Polarity of ZrBTC-A and ZrBTC-AE2 MOFs.

Supplementary References

1.	Shearer, G.C., et al., *Defect Engineering: Tuning the Porosity and Composition of the Metal–Organic Framework UiO-66 via Modulated Synthesis.* Chemistry of Materials, 2016. **28**(11): p. 3749-3761.

2.	Antoine, M.D., S. Devanathan, and G. Patonay, *Determination of critical micelle concentration of surfactants using a near-infrared hydrophobicity probe.* Microchemical Journal, 1991. **43**(2): p. 165-172.

3.	Carolina, A.-S., et al., *An Analysis of the Effect of the Zirconium Precursor of MOF-808 on Its Thermal, Structural, and Surface Properties*. 2018.

4.	Pan, D., M. Jaroniec, and J. Klinik, *Thermogravimetric evaluation of the specific surface area and total porosity of microporous carbons.* Carbon, 1996. **34**(9): p. 1109-1113.

5.	Araujo, A.S. and M. Jaroniec, *Determination of the surface area and mesopore volume for lanthanide-incorporated MCM-41 materials by using high resolution thermogravimetry.* Thermochimica Acta, 2000. **345**(2): p. 173-177.

6.	Furukawa, H., et al., *Water Adsorption in Porous Metal–Organic Frameworks and Related Materials.* Journal of the American Chemical Society, 2014. **136**(11): p. 4369-4381.

7.	James, J.B. and Y.S. Lin, *Kinetics of ZIF-8 Thermal Decomposition in Inert, Oxidizing, and Reducing Environments.* The Journal of Physical Chemistry C, 2016. **120**(26): p. 14015-14026.

8.	Liang, W., et al., *Tuning pore size in a zirconium-tricarboxylate metal-organic framework.* CrystEngComm, 2014. **16**(29): p. 6530-6533.

9.	Ardila Suárez, C., et al., *An Analysis of the Effect of the Zirconium Precursor of MOF-808 on its Thermal Stability, Structural and Surface Properties.* CrystEngComm, 2019.

10.	Mukerjee, P. and K.J. Mysels, *Critical micelle concentrations of aqueous surfactant systems*, 1971, National Standard reference data system.

11.	Zhang, Q., et al., *A porous metal–organic framework with –COOH groups for highly efficient pollutant removal.* Chemical Communications, 2014. **50**(92): p. 14455-14458.

12.	Piszczek, P., et al., *The new type of [Zr6(μ3-O)4(μ3-OH)4] cluster core: Crystal structure and spectral characterization of [Zr6O4(OH)4(OOCR)12] (R=But, C(CH3)2Et).* Polyhedron, 2007. **26**(3): p. 679-685.

13.	Ardila Suárez, C., et al., *Synthesis, Characterization, and Post-Synthetic Modification of a Micro/Mesoporous Zirconium-Tricarboxylate Metal-Organic Framework: Towards the Addition of Acid Active Sites.* CrystEngComm, 2019.